Bone 117 (2018) 130–137

Contents lists available at ScienceDirect

Bone

journal homepage: www.elsevier.com/locate/bone

Full Length Article

Examining the influence of PTH(1-34) on tissue strength and composition☆

Joseph D. Gardinier[a], Salam Al-Omaishi[b], Niloufar Rostami[a], Michael D. Morris[c], David H. Kohn[b,d,*]

[a] Bone and Joint Center, Henry Ford Hospital, Detroit, MI 48202, USA
[b] Department of Biomedical Engineering, University of Michigan, Ann Arbor, MI 48109, USA
[c] Department of Chemistry, University of Michigan, Ann Arbor, MI 48109, USA
[d] Department of Biologic and Materials Sciences, University of Michigan, Ann Arbor, MI 48109, USA

ARTICLE INFO

Keywords:
PTH(1-34)
Perilacunar remodeling
Raman spectroscopy
Microdamage

ABSTRACT

The lacunar-canaliculi system is a network of channels that is created and maintained by osteocytes as they are embedded throughout cortical bone. As osteocytes modify their lacuna space, the local tissue composition and tissue strength are subject to change. Although continual exposure to parathyroid hormone (PTH) can induce adaptation at the lacunar wall, the impact of intermittent PTH treatment on perilacunar adaptation remains unclear. Therefore, the primary objective of this study was to establish how intermittent PTH(1-34) treatment influences perilacunar adaptation with respect to changes in tissue composition. We hypothesized that local changes in tissue composition following PTH(1-34) are associated with corresponding gains in tissue strength and resistance to microdamage at the whole bone level. Adult male C57BL/6J mice were treated daily with PTH (1-34) or vehicle for 3 weeks. In response to PTH(1-34), Raman spectroscopy revealed a significant decrease in the carbonate-to-phosphate ratio and crystallinity across the entire tissue, while the mineral-to-matrix ratio demonstrated a significant decrease in just the perilacunar region. The shift in perilacunar composition largely explained the corresponding increase in tissue strength, while the degree of new tissue added at the endosteum and periosteum did not produce any significant changes in cortical area or moment of inertia that would explain the increase in tissue strength. Furthermore, fatigue testing revealed a greater resistance to crack formation within the existing tissue following PTH(1-34) treatment. As a result, the shift in perilacunar composition presents a unique mechanism by which PTH(1-34) produces localized differences in tissue quality that allow more energy to be dissipated under loading, thereby increasing tissue strength and resistance to microdamage. In addition, our findings demonstrate the potential for PTH(1-34) to amplify osteocytes' mechanotransduction by producing a more compliant tissue. Overall, the present study demonstrates that changes in tissue composition localized at the lacuna wall contribute to the strength and fatigue resistance of cortical bone gained in response to intermittent PTH(1-34) treatment.

1. Introduction

The mechanical strength of bone is a function of its hierarchical structure that spans across various length scales, ranging from nanometers to centimeters [1]. At the micron scale, the lacunar-canaliculi system is a network of channels that is created and continually maintained by osteocytes as they are embedded in bone [2–4]. The capacity for osteocytes to modify or restructure the lacuna in particular was first observed over 100 years ago in patients with rickets and osteomalacia based on the enlarged lacunae present throughout their cortical bone [5,6]. In more recent studies, osteocytes have also been shown to modify the canaliculi in a similar manner as the lacuna [7]. Adaptation of the lacuna void has been documented under numerous conditions that include lactation, diabetes, exercise, micro-gravity, and aging [7–15]. However, the impact that lacuna adaptation has on tissue composition and strength is relatively unknown.

Adaptation of the lacuna is readily facilitated through parathyroid hormone (PTH) and PTH-related protein (PTHrP) activation of the PTH/PTHrP receptor (PPR). Under continuous PTH treatment, the lacuna void is significantly enlarged, with a higher presence of immature matrix that is less mineralized [16]. Similarly, elevated levels of PTHrP that are sustained during lactation enlarge the lacuna volume as

☆ Funding sources: NIH DE07057 (DHK), AR056657 (DHK), AR064668 (JDG).
* Corresponding author at: Dept. of Biological and Material Sciences, 2213 School of Dentistry, University of Michigan, Ann Arbor, MI 48109-1078, USA.
E-mail address: dhkohn@umich.edu (D.H. Kohn).

https://doi.org/10.1016/j.bone.2018.09.019
Received 29 May 2018; Received in revised form 27 August 2018; Accepted 23 September 2018
Available online 24 September 2018
8756-3282/

calcium is sequestered from the surrounding mineral for milk production [7,12]. Upon removal of PTH, the lacuna wall undergoes mineralization, constricting the lacuna space [12,16]. In contrast to continuous PTH treatment, very little is known regarding the impact of intermittent PTH treatment on the adaptation of the lacuna void and its surrounding tissue. In the context of exercise, the transient release of endogenous PTH increased the presence of new, immature mineral at the lacuna wall with higher carbonate content [14]. The coinciding lack of change in lacuna size, suggested the new mineral was replacing tissue previously removed at the onset of exercise. However, given that exercise produces other forms of stimuli that effect osteocyte behavior, it remains unclear to what extent intermittent PTH treatment alone influences lacunar adaptation. In particular, changes in lacuna size and its surrounding tissue composition can provide valuable insight on how intermittent PTH treatment enhances the mechanical behavior of bone.

The chemical composition of bone is a key determinate of tissue strength [17]. Bone strength and toughness gained by altering the tissue composition can occur at various length scales. For example, new tissue added through modeling or remodeling in response to PTH(1-34) can decrease the average age of the tissue [17,18]. In contrast, local changes in tissue composition and modulus at the micro and nano scales provide a toughening mechanism by limiting crack growth [17,19–21]. Adaptation at the lacuna wall in particular, has the capacity to either increase or decrease the spatial variation in tissue composition. However, the impact that local variations in tissue composition have on whole bone mechanics remains unclear.

Under conventional intermittent PTH(1-34) treatment, gains in tissue strength have been attributed to bone turnover and gains in bone mass [22,23]. In contrast, treating mature mice for only 3-weeks with PTH(1-34) provides minimal changes in bone mass that do not explain the corresponding increase in tissue strength. Therefore, the primary objective of this study was to examine after 3-weeks of PTH(1-34) treatment the changes in tissue composition and lacuna size in relation to changes in tissue strength. We hypothesized that local changes in tissue composition following PTH(1-34) are associated with corresponding gains in tissue strength and resistance to microdamage at the whole bone level. Overall, our data demonstrate that intermittent PTH (1-34) decreases the perilacunr mineral-to-matrix ratio and carbonate-to-phosphate ratio, and that this shift in perilacunar composition correlates with an increase in tissue strength.

2. Methods

2.1. In-vivo protocols

Animal procedures were performed at the University of Michigan with University Committee on Use and Care of Animals (UCUCA) approval. To avoid confounding effects from endogenous changes in PTH levels due to menstruation [24], male C57BL/6J mice were purchased from Jackson Laboratories (Bar Harbor, ME), at 15 weeks of age and allowed to acclimate in individual housing with sufficient water, food, and items for enrichment. At 16-weeks of age, mice were divided into two weight-matched groups with 7 mice in each group: vehicle and PTH(1-34). Each group received daily subcutaneous injections of either 50 μl of saline solution (0.9% NaCl) as a vehicle control, or 40 μg/kg of hPTH(1-34) (Bachem, CA) in saline. Mice received fluorochrome injections at day 3 (alizarin complexone, 25 mg/kg) and day 15 (xylenol orange, 90 mg/kg). The fluorochrome markers were used to quantify the apposition of mineralized tissue and percentage of new cortical tissue added under each treatment. Each mouse was then sacrificed on day 21 to isolate the tibiae and femora, which were then wrapped in gauze soaked with Ca^{2+} buffered saline and stored at −80 °C until further use. The right tibiae were used for μCT analysis and monotonic mechanical testing, while the left tibiae were used for Raman spectroscopy. In addition, the right femora were used for fatigue testing and microdamage analysis, while the left femora were used as the non-fatigued control for microdamage analysis.

2.2. Micro-computed tomography (μCT) analysis

Prior to any mechanical loading, the tibiae and femora were scanned in a Scanco μCT system (μCT100 Scanco Medical, Bassersdorf, Switzerland) with the following settings: 12 μm voxel size, medium resolution, 70 kVp, 114 μA, 0.5 mm AL filter, 500 ms integration time. For each scan, samples were embedded in 1% agarose, to prevent dehydration. Image slices were processed with a greyscale threshold optimized across the entire population of samples.

Images of each tibia were orientated to match their position during mechanical testing. A standard site was defined in the mid-diaphysis, midway between the loading points, while the fracture site was defined based on the distance between the distal tibia-fibula junction and where the crack initiated along the medial side under tension. At both sites the cortical bone thickness, cross-sectional area, bone mineral content (BMC), bone mineral density (BMD), distance from the neutral axis to the most medial surface, moment of inertia about the anterior-posterior axis ($MOI_{A/P}$) and medial-lateral axis ($MOI_{M/L}$) were determined. The parameters at the fracture site were used to estimate tissue-level mechanical properties, while the means and standard errors from the standard site are reported.

Images of each femur were also orientated to match their position during the fatigue test. A standard cortical site was defined midway between the loading points where the moment of inertia about the medial-lateral axis ($MOI_{M/L}$) and distance to the neutral axis were determined for calculating the needed force for fatigue testing.

2.3. Histomorphometry

The purpose of the fluorochrome labels was to quantify the amount of mineralized tissue formed during treatment as a percentage of the total cortical area. First, each tibia was embedded in methyl methacrylate (Koldmount Cold Mount kit, Mager Scientific, MI) following graded ethanol dehydration. Sections were then cut at the mid-diaphysis using a low-speed sectioning saw (South Bay Technology, Model 650, CA) with a diamond wafering blade (Mager Scientific, MI), and polished on wet silicon carbide abrasive disks to a final thickness of 100 μm. Fluorochrome labels were identified under a confocal microscope (Olympus FluoView™ FV1000) to calculate the mineralizing surfaces (MS) as a percentage of the endosteum and periosteum surfaces according to standardized histomorphometric analysis using ImageJ software [25]. In addition, new tissue was defined by the area between the alizarin red label and endosteal or periosteum surface. Regions that contained only xylene labels given on day 15 were also included to calculate new tissue content. For each sample, the total new tissue was normalized to total bone area.

2.4. Raman spectroscopy and lacuna size

Raman spectroscopy was used to evaluate the tissue composition localized around individual lacuna in comparison to composition away from the lacunar wall. Tibiae sections prepared for histomorphometry were used since the samples were not fixed in formalin, but only dehydrated over the course of 24 h in a series of graded ethanol washes prior to embedding in methyl methacrylate. Sections of each tibia were imaged using a Raman microprobe with a 785-nm diode laser (Invictus, Kaiser Optical Systems) and a line focused laser beam (60 μm in length) through a polarization scrambler and a 40×/0.75 N objective (S Fluor, Nikon Instruments) with a diffraction limitation of ~500 nm based on the objective and its numerical aperture of 0.9. The Raman spectra were collected over the perilacunar and non-perilacunar regions as previously described [14]. Briefly, distances along the laser line were first calibrated. The laser line was then positioned to extend out from the lacuna wall. Hyperspectral Raman images were taken at each position

along the laser line. Images within 0–5 μm from the lacuna wall were averaged to characterize the perilacunar tissue, while images within 10–15 μm from the lacuna wall were averaged to characterize non-perilacunar tissue. Image data was then processed as described [26,27]. A peak fitting routine was used to identify peak intensities for phosphate (959 cm^{-1}), carbonate (1070 cm^{-1}), and the hydroxyprolines (851 cm^{-1} and 873 cm^{-1}) as the matrix phase. The phosphate peak was then used to normalize the image. The mineral-to-matrix ratio (MMR) was calculated as 959 cm^{-1}/(851 cm^{-1} and 873 cm^{-1}), and the carbonate-to-phosphate ratio (CPR) was calculated as 1070 cm^{-1}/958 cm^{-1}. The crystallinity was defined by the inverse of the phosphate band width at half of the maximum intensity (1/FWHM 958 cm^{-1}). Lacunae were randomly selected from the medial region of the tibiae and their cross-sectional areas were measured along with each Raman parameter. Each parameter was averaged across 3 to 4 imaged lacunae taken from the same sample. A total of 7 samples were tested for each group and the mean and standard error for each group are reported.

2.5. Monotonic fracture test

The mechanical properties of each tibia scanned for μCT analysis were determined under four-point bending using an Admet eXpert 450 Universal Testing Machine [28]. The base support span was 9 mm with a loading span of 3 mm. The tibia was positioned in the loading device, such that the medial surface was in tension by placing the most distal portion of the tibia and fibula junction directly over the left-most support point. Each tibia was loaded at a rate of 0.01 mm/s until failure, while the load and displacement were recorded. The force displacement curve was used to determine structural-level mechanical properties. The following beam bending equations for four-point loading were then used to estimate the tissue-level mechanical properties:

$$\text{Stress} = \sigma = f \bullet a \bullet c/2 \bullet \text{MOI}_{\text{A/P}}$$

$$\text{Strain} = \varepsilon = 6 \bullet c \bullet d/a(3 \bullet L - 4 \bullet a)$$

In each equation, f is the applied force, d is the resulting displacement, a is the distance between the inner spans (3 mm), L is the distance of the outer spans (9 mm), and c is the distance from the neutral axis to the surface under tension. Since the cylindrical shape at the mid-diaphysis of the tibia begins to collapse after the yield point, beam bending equations were only used to measure the yield and ultimate stress strain properties alongside the modulus of elasticity. The yield point was determined from the stress-strain relationship using a 20% offset method [29].

2.6. Fatigue test

The resistance to microdamage was tested by subjecting the right femora to cyclic loading. First a pre-loading phase was applied under a sinusoidal profile of 2 Hz for 20 cycles between 0 and 5 N using a Bose® EnduraTech ELF 3200 Series device. The force deflection curve was then used to estimate the modulus using the geometric properties identified under μCT. The required load needed to produce a peak strain of 10,000 micro-strain along the anterior surface was then calculated and applied over 40,000 cycles at 2 Hz. At this level of strain, the applied stress was ~50 MPa for vehicle treated samples and ~80 MPa for PTH(1-34) samples, both of which are 30% or more below the yield point of age-matched vehicle treated controls. The use of such high strains was chosen to examine how much PTH(1-34) is able to reduce the level of damage. All testing was conducted in a 37 °C calcium-buffered saline solution.

The fatigued and non-fatigued contralateral femora were stained with basic fuchsin in a graded ethanol dehydration (70, 80, 90, 100%), then embedded in PMMA and sectioned as described earlier. Each section was imaged using a confocal microscope (Olympus FluoView™ FV1000). Microdamage was evaluated in the anterior region of both loaded and non-loaded femora by quantifying the area of diffuse damage, and the number and length of linear cracks [30]. Diffuse damage was identified as a pooling of fuchsin staining that was > 300 μm^2 (average area of 3 lacuna). Linear cracks < 10 μm in length were not counted. Values of diffuse damage and crack number were normalized to the total cortical area in each image.

2.7. Statistical analysis

All outcome measures are reported as the group mean ± the standard error of mean. Using SPSS, normality was first verified using a Shapiro-Wilk test. Next, a single classification analysis of variance (ANOVA) was performed to calculate statistical differences in lacuna area, cortical geometry, histomorphometry, and mechanical properties between vehicle and PTH(1-34) treatments. For tissue composition, the main and interaction effects of treatment (vehicle vs. PTH) and region of interest (perilacunar vs. non-perilacunar) were evaluated using a two-factor analysis of variance (ANOVA) with repeated measures and Tukey post-hoc testing between groups. Measures of microdamage were also evaluated for main and interaction effects of treatment and limb (loaded vs. non-loaded) using the same two-way ANOVA. Differences between the initial and final stiffness and modulus for the femur were evaluated using a paired Student t-test. The relationship between tissue composition and whole bone strength was then evaluated by calculating the Pearson's correlation coefficients. Throughout the study, a p-value < 0.05 was considered significant.

3. Results

3.1. Perilacunar composition is modified following PTH(1-34) treatment

Following 3-weeks of PTH(1-34) or vehicle treatment, tissue composition of the tibia was evaluated across both perilacunar and non-perilacunar regions using Raman spectroscopy. Relative position to the lacuna wall (e.g. perilacunar versus non-perilacunar tissue) had a significant main effect on the mineral-to-matrix ratio ($p = 0.02$), which was driven by the significant decrease in this ratio in perilacunar vs. non-perilacunar tissue in PTH(1-34) treated samples (Fig. 1A). The carbonate-to-phosphate ratio and crystallinity were significantly dependent on treatment ($p < 0.001$), with both the carbonate-to-phosphate ratio and crystallinity being significantly decreased by PTH(1-34) treatment (Fig. 1B & C). The cross-sectional area of each lacuna imaged was on average 13 larger and significantly greater in the PTH(1-34) treated group compared to vehicle treated group (Fig. 1D).

3.2. PTH(1-34) modifies the structural-level and tissue-level mechanical properties of bone

Having identified key changes in tissue composition following PTH (1-34) treatment, both structural-level and tissue-level mechanical properties were then evaluated in the contralateral limb. At the structural-level, there was a significant increase in the stiffness of tibiae from PTH(1-34) treated mice, while tissue-level mechanical properties revealed a significant increase in modulus and ultimate stress and significant decrease in yield strain. Based on μCT analysis, the tibiae displayed insignificant differences in cortical area, thickness, bone mineral density, and moment of inertia compared to vehicle treated controls (Table 1). Imaging of the fluorochrome labels demonstrated that 24% of the endosteal and periosteal surfaces were mineralizing following PTH (1-34) treatment compared to only 10% in the vehicle treated controls ($p < 0.05$, Table 1; Fig. 2). The BFR was also significantly increased following PTH(1-34) treatment. Only 2.5% of the cortical area in PTH (1-34) treated samples was identified as new tissue compared to 1.8% in the vehicle control; however, the difference in new formed tissue was not statistically significant.

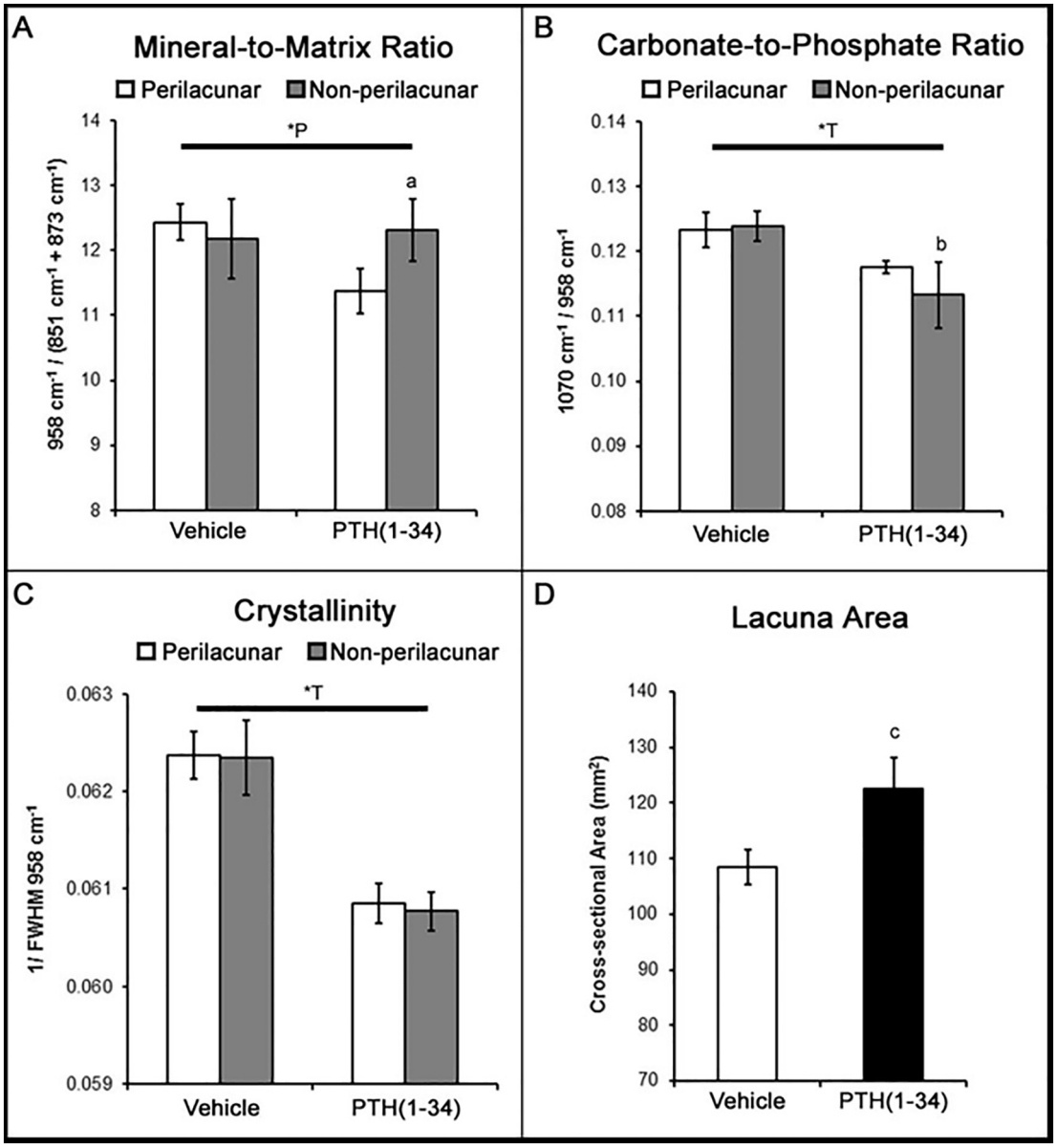

Fig. 1. Tissue composition based on Raman spectroscopy revealed significant changes in both perilacunar and non-perilacunar regions following PTH(1-34) treatment. PTH(1-34) reduced the perilacunar mineral-to-matrix ratio (A), while reducing the carbonate-to-phosphate (B), and crystallinity (C) across both regions. D) Lacuna cross-sectional area was significantly larger in the PTH(1-34) treated group. Significant main factor effects are noted for treatment (*T), relative position to lacuna wall (*P), or their interaction (*TxP). Tukey post hoc analysis of specific group differences with a p-value < 0.05 are noted by 'a' for comparisons between region and 'b' for comparisons between treatment. 'c' indicates p-value < 0.05 between vehicle and PTH(1-34) treated groups. Mean ± sem are shown (n = 7, each n represents 3 to 4 lacuna from each sample).

3.3. PTH(1-34) increases the resistance to microdamage

Given the influence that PTH(1-34) had on the tissue-level mechanical properties, we then evaluated the ability of PTH(1-34) to increase resistance to microdamage under fatigue loading. During fatigue loading, the vehicle group displayed a significant loss in stiffness (118 ± 6.1 N/mm initial vs. 88 ± 8.7 N/mm final; $p < 0.001$) and modulus (7.8 ± 0.7 GPa initial vs. 5.8 ± 0.7 GPa final, $p < 0.001$) based on paired Student *t*-tests. PTH(1-34) treated samples also displayed a significant loss in stiffness (137 ± 5.0 N/mm initial vs. 112 ± 4.5 N/mm final; $p < 0.001$) and modulus (8.5 ± 0.6 GPa initial vs. 6.9 ± 0.5 GPa final; $p < 0.001$). Although the percent loss in stiffness for the vehicle group was higher than for the PTH(1-34) group, it was not statistically significant (−26 ± 4.8% vehicle vs. −18 ± 2.7% PTH(1-34), $p = 0.09$).

After fatigue loading, the presence of micro-cracks and diffuse damage was significantly less in PTH(1-34) treated samples (Fig. 3). Crack density was significantly dependent on fatigue loading ($p = 0.05$) and treatment ($p = 0.05$). In addition, there was a significant interaction between treatment and loading on crack density ($p = 0.001$). Post hoc analysis found fatigue loading significantly increased crack density in the vehicle group, but not the PTH(1-34) treated group. Treatment also had a main effect on the linear crack length ($p = 0.05$) and diffuse damage density ($p = 0.04$). In particular, diffuse damage for both fatigued and non-fatigued conditions was significantly lower in PTH(1-34) treated groups compared to vehicle treated groups. Altogether, fatigue loading increased crack density, but not crack length, indicating that loading led to an increase in crack nucleation, but not crack growth. PTH prevented new cracks or diffuse damage from forming under cyclic loading, but did not have a significant effect on crack

Table 1
Mouse body weights, structural geometry, histomorphometry, and mechanical properties of the tibia in response to vehicle and PTH(1-34) treatments.

	Vehicle Mean (sem)	PTH(1-34) Mean (sem)
Change in body weight (gm)	26.1 (1.5)	26.5 (1.5)
Geometric properties		
Cortical area (mm^2)	0.73 (0.02)	0.79 (0.02)
$MOI_{M/L}$ (mm^4)	0.09 (0.01)	0.09 (0.01)
$MOI_{A/P}$ (mm^4)	0.16 (0.01)	0.18 (0.01)
Distance to neutral axis (mm)	0.60 (0.02)	0.62 (0.01)
Bone mineral density (mg/cm^2)	1201 (10)	1202 (12)
Bone mineral content (mg)	147.6 (4.7)	158.8 (5.3)
Histomorphometry		
MS/BS (μm/μm)**	0.098 (0.012)	0.240 (0.040)
MAR (μm/day)	1.02 (0.194)	1.07 (0.106)
BFR (μm/μm/day)**	0.085 (0.011)	0.290 (0.064)
New tissue (% of cortical area)	1.90 (0.01)	2.55 (0.01)
Structural-level properties		
Yield load (N)	17.94 (0.9)	19.85 (1.2)
Yield displacement (mm)	269.1 (15.4)	237.1 (10.7)
Stiffness (N/mm)**	77.2 (6.11)	94.9 (5.15)
Ultimate load (N)	18.37 (0.7)	20.39 (1.3)
Post-yield displacement (mm)	110.2 (10.6)	160.7 (40.0)
Tissue-level properties		
Yield stress (MPa)*	180.7 (9.0)	203.3 (8.7)
Yield strain (MPa)**	21,910 (1199)	19,072 (384)
Modulus (GPa)**	9.46 (0.56)	12.02 (0.33)
Ultimate stress (MPa)**	184.8 (7.5)	208.6 (8.0)

* p-Value < 0.1.
** p-Value < 0.05.

growth.

3.4. Coordinated changes in perilacunar composition and tissue strength

The potential influence that local changes in mineral composition may have on the tissue-level mechanical properties was evaluated by calculating the Pearson Correlation Coefficients between the whole bone mechanical properties and the composition of perilacunar and non-perilacunar tissue (Table 2). There was a significant negative relationship between perilacunar MMR and yield stress, indicating that a decrease in the perilacunar MMR corresponds with an increase in yield stress (Fig. 4). There was also found a significant negative correlation between perilacunar CPR and ultimate stress. There were no significant relationships between any geometric property (cortical area, moment of inertia, mineral content, or bone mineral density) and tissue-level mechanical properties.

4. Discussion

The present study demonstrates a unique mechanism by which intermittent PTH(1-34) treatment improves tissue strength and resistance to microdamage by facilitating changes in the tissue composition localized at the lacuna wall. Based on spatially localized Raman spectroscopy, the response to PTH(1-34) is characterized by a decrease in the mineral-to-matrix ratio at the lacuna wall, along with decreases in the carbonate-to-phosphate ratio and crystallinity that extend beyond the perilacunar zone (Fig. 1). At the whole bone level, PTH(1-34) treatment increased stiffness despite insignificant changes in bone mass (i.e. cortical area, bone mineral content) and cross-sectional geometry (i.e. cortical thickness, moment of inertia, distance to the neutral axis) (Table 1). The increase in structural level properties corresponded with a significant increase in modulus and tissue strength (and ultimate-stress). In addition to whole bone mechanical properties, PTH(1-34) treatment also increased the resistance to microdamage (Fig. 3), further suggesting an adaptation in the existing tissue composition. Overall, the gains in tissue strength and resistance to microdamage following PTH (1-34) treatment are not fully explained by bulk changes in bone mass or geometry, but are a function of changes in the existing tissue composition. The correlation between tissue strength and perilacunar composition represents a unique mechanism by which localized adaptation can influence tissue strength.

Treating mature mice intermittently with PTH(1-34) for only 3-weeks demonstrated a unique capacity to increase tissue strength without requiring significant changes in bone mass or geometry. On average, PTH(1-34) increased tissue strength by 12% and increased the stiffness and modulus by 22% (Table 1). In contrast, cortical area increased by 7% in response to PTH(1-34), while the moment of inertia and distance to the neutral axis under bending increased by 5% and 3% respectively. None of these increases were statistically significant. Changes in cortical area and cross-sectional geometry equal to those incurred in response to PTH(1-34) treatment would then only account for an 8% increase in the applied stress for a given bending load. Thus, the gains in tissue strength were considered driven, at least in part, by

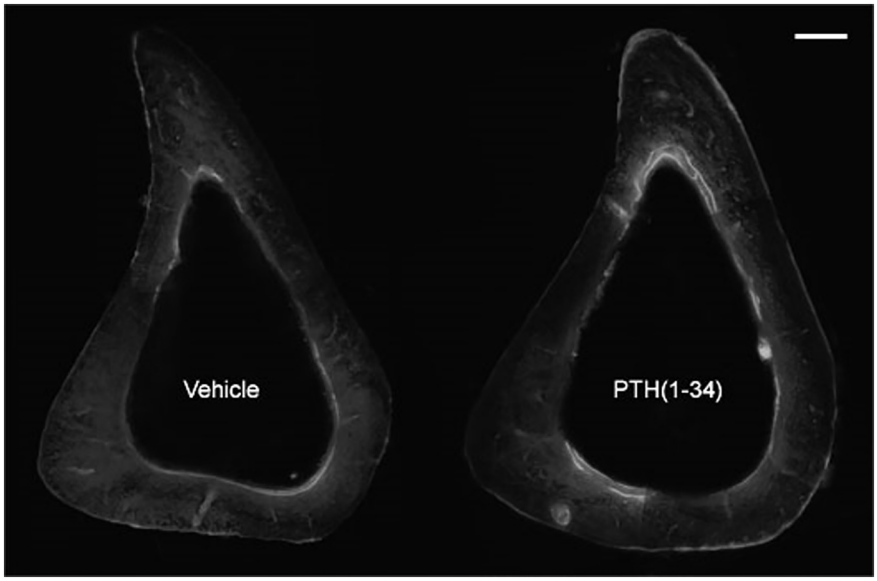

Fig. 2. Micrographs of a representative tibia show greater double labeling along the endosteum and periosteum following 3-weeks of intermittent PTH(1-34) treatment, yet no significant change in cortical area or moment of inertia. Scale bar is 250 μm.

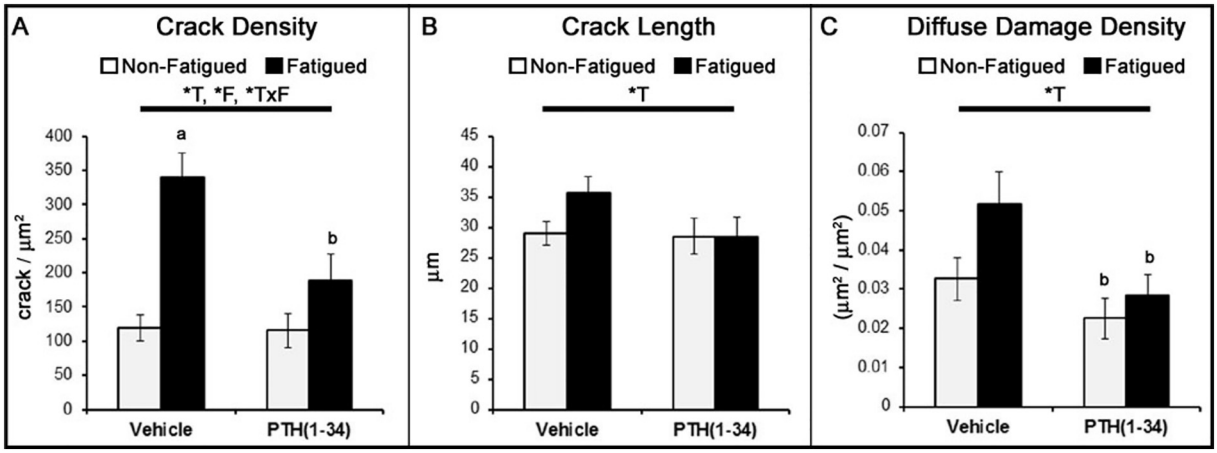

Fig. 3. Microdamage following cyclic loading was significantly reduced by PTH(1-34) treatment. The crack density (A), linear crack length (B), and diffuse damage density (C) were quantified in both non-fatigued and fatigued limbs. In vehicle treated samples, fatigue loading significantly increased crack density, but this increase did not occur in the PTH(1-34) treated group. Treatment had a main effect on linear crack density and length and the diffuse damage density. Significant main factor effects are noted for treatment (*T), fatigue (*F), and their interaction (*TxF). Tukey post hoc analysis of specific group differences with a p-value < 0.05 are noted by 'a' for loaded vs. non-loaded comparisons, and 'b' for vehicle vs. PTH(1-34) comparisons. Mean ± sem are shown (n = 7).

Table 2
Pearson's correlation coefficients between whole bone mechanics and the tissue composition metrics of perilacunar and non-perilacunar regions.

	Perilacunar		Non-perilacunar	
	Mineral-to-matrix	Carbonate-to-phosphate	Mineral-to-matrix	Carbonate-to-phosphate
Yield stress	−0.462**	−0.496*	0.019	0.035
Yield strain	0.503**	0.175	0.445	0.067
Modulus	−0.515**	−0.464*	−0.220	−0.076
Ultimate stress	−0.441*	−0.519**	0.022	−0.148

* p-Value < 0.1.
** p-Value < 0.05.

changes in the existing tissue or the type of tissue formed along the surfaces in response to PTH(1-34).

Within the existing tissue, intermittent PTH(1-34) treatment caused a significant decrease in perilacunar mineral-to-matrix ratio, while decreasing the carbonate-to-phosphate ratio and crystallinity across both perilacunar and non-perilacunar regions. Based on our findings, the variation in tissue strength was in part explained by changes in perilacunar composition. In particular, a decrease in both mineral-to-matrix ratio and carbonate-to-phosphate ratio correlated with an increase in tissue strength and modulus (Fig. 4). The inverse relationship between tissue strength and carbonate-to-phosphate ratio is consistent with clinical findings where reduced tissue strength among older adults and individuals with osteoporosis is characterized by increased carbonate-to-phosphate ratio [17,18,31–35]. Less carbonate substitution into the mineral produces fewer vacancies in the lattice structure that would compromise tissue strength. In general, the fewer vacancies and imperfections within the lattice structure created by carbonate substitution would increase the crystallinity. However, crystallinity is also a function of the crystallite dimension and its length along the c-axis [31,36]. As a result, the impact of carbonate substitution on crystallinity can be offset due to changes in crystallite growth. This has been shown to occur with aging, where both carbonate substitution as well as crystal size along the c-axis increase, and together explain a lack of change in crystallinity [31,37–39]. Based on our findings, the decrease in crystallinity following PTH(1-34) is considered more a function of changes in the crystallite size than the decrease in carbonate substitution. Given that PTH induces expression of various non-collagenous proteins that reduce mineral growth and maturation, differences in crystal size would not be unexpected between treated and non-treated groups [40]. Modifications to both carbonate substitution and crystallinity across both perilacunar and non-perilacunar tissue tells us that the effects of PTH(1-34) are not limited to only new tissue being deposited or existing tissue exposed to active cells.

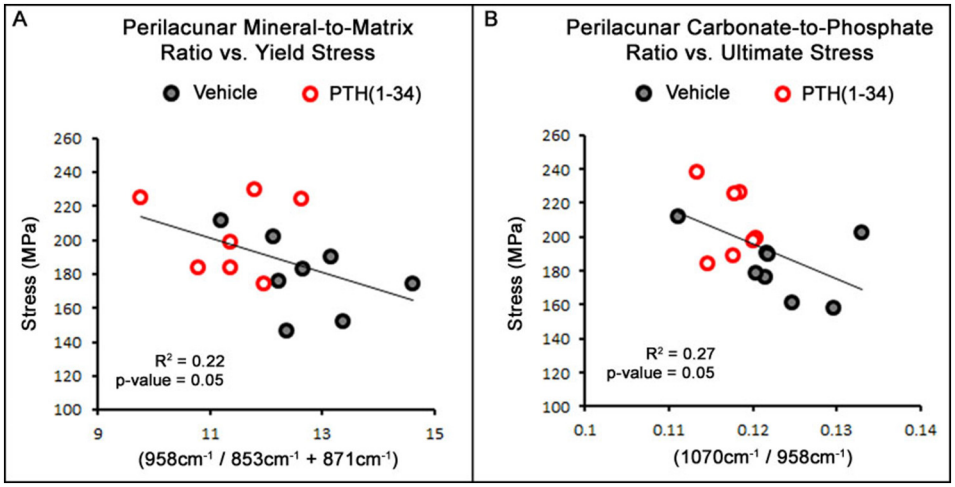

Fig. 4. The perilacunar mineral-to-matrix ratio and carbonate-to-phosphate ratio correlated with tissue-level strength, yield stress and ultimate stress respectively. A) The perilacunar mineral-to-matrix ratio exhibited a significant relationship with yield stress, indicating that a loss in mineral-to-matrix ratio at the lacuna wall corresponds with gains in tissue strength. B) The perilacunar carbonate-to-phosphate ratio displayed a significant negative relationship with ultimate stress.

Contrary to expectation, our findings also demonstrated an inverse relationship between the perilacunar mineral-to-matrix ratio and tissue strength. However, it's unclear if the decrease in mineral-to-matrix ratio due to PTH(1-34) was due to mineral being removed from the tissue, or the deposition of new matrix to replace that previously removed to enlarge the lacuna void. Considering that lacuna size increased in response to PTH(1-34), we suspect mineral is being removed in response to intermittent PTH(1-34). In either case, a decrease in perilacunar mineral-to-matrix ratio indicates a more compliant tissue. The corresponding increase in tissue strength as the perilacunar tissue becomes more compliant is then likely a function of the resulting difference between perilacunar and non-perilacunar composition. Differences between perilacunar and non-perilacunar composition would allow a greater degree of energy to be dissipated throughout tissue under loading. Conversely, bone in which the mineral-to-matrix ratio is more homogenous has a greater fracture risk [31,41,42]. The increasing difference between perilacunar and non-perilacunar mineral-to-matrix ratio following PTH(1-34) treatment would also explain the increased resistance to microdamage during fatigue loading. Spatial variations in tissue composition play a key role in crack formation and propagation through bone [43,44]. Several studies have found that micro-cracks and microdamage originate at the lacuna wall [45–48]. Thus, by producing a more compliant tissue at the lacuna wall, more energy is allowed to dissipate under loading, resulting in greater resistance to microdamage alongside an overall increase in tissue strength.

In addition to tissue strength, a more compliant perilacunar tissue will also increase the degree of strain generated at the lacuna wall, where osteocytes' interface with the extracellular matrix. Bonivtch et al. (2007) reported that a more complaint perilacunar tissue increases the local strain magnitudes; thus subjecting osteocytes to larger mechanical stimuli under dynamic loading [49]. As a result, local changes in tissue composition following PTH(1-34) treatment have the potential to enhance mechanotransduction indirectly by augmenting the mechanical stimuli osteocytes experience during physical activity. This is consistent with the additive effect PTH(1-34) treatment on bone adaptation during in-vivo loading or treadmill exercise [50–52]. However, the additive effect provided by PTH(1-34) treatment is readily considered a function of PTH altering the cellular response to mechanical stimuli as well as its down-stream activation of similar anabolic mechanisms [53,54]. Changes in tissue compliance have largely been ignored and warrant further investigation regarding their impact on mechanotransduction.

Adaptation of the existing tissue was also accompanied by an increase in mineralization along both endosteal and periosteal surfaces in response to PTH(1-34). The increase in mineral apposition resulted in an increased bone formation rate (Table 1). However, the increases in MS/BS and BFR did not produce a significant increase in cortical area or moment of inertia. Based on double labeling, PTH(1-34) treatment increased the percentage of tissue undergoing mineralization by ~14% (0.098 vs. 0.24, Table 1). Assuming an average of 650 lacuna/mm^2 with each lacuna averaging an elliptical cross-section 5 μm wide and 7 μm long [55], the 14% increase in mineralizing surfaces in response to PTH (1-34) is equivalent to the same surface area that 6% of the osteocytes are exposed to. As a result, perilacunar adaptation over a small portion of bone's cortex is likely to affect more surface area than that being modified at the endosteum and periosteum. However, this does not dismiss the possibility that the type of tissue formed along the surfaces in response to PTH(1-34) may present differences in composition that would influence tissue strength. In mice, tissue that is formed in response to PTH(1-34) treatment exhibits a lower crystallinity, but similar mineral-to-matrix ratio and carbonate-to-phosphate ratio as new tissue formed under normal conditions [56]. Given that the percentage of new tissue added in response to PTH(1-34) was not statistically greater than vehicle controls, and combined with their expected similarities in composition, the increase in bone strength was considered to more a function of changes in the existing tissue.

The increased resistance to microdamage following PTH(1-34) is consistent with previous reports in sheep [22,23]. However, in osteonal bone, the formation and extension of micro-cracks are primarily dictated by larger architectural structures, such as the haversian canals and cement lines [30,48]. As a result, the use of larger animal models is required to verify how perilacunar adaptation influences tissue strength relative to the larger structures in osteonal bone. Despite this limitation, our study demonstrates the potential for perilacunar adaptation to enhance tissue strength without requiring significant gains in bone mass, which is difficult to invoke in aged or diseased patients. Another limitation in this study is our lack of information regarding the matrix phase, such as collagen crosslinking and protein composition (collagenous and non-collagenous). Even with adequate resolution, the amide I band contained too much noise to accurately identify the 1690 and 1660 peaks often associated with collagen cross-link maturation [17,18]. At the cellular level, osteocytes expression of collagenous and non-collagenous proteins in response to PTH can have significant implications on the matrix structure or mineralization [57,58]. For example, the presence of osteopontin or osteocalcin in the matrix phase can have a large influence on the mechanical strength and toughness of the matrix [59,60]. Overall, our findings warrant further investigation to understand how PTH influences the perilacunar matrix composition, as well as the composition localized around larger structures that may also influence tissue strength and crack resistance.

In summary, our findings demonstrate that intermittent PTH(1-34) treatment produces significant changes in both perilacunar and non-perilacunar tissue composition. Furthermore, the corresponding increase in tissue strength is explained by the shift in perilacunar tissue composition. The negative relationship between perilacunar mineral-to-matrix ratio and tissue strength suggests a unique mechanism by which PTH(1-34) treatment allows more energy to be dissipated at the lacuna wall under loading, thereby reducing the formation of microdamage under fatigue loading. The shift in perilacunar composition also suggests a potential mechanism by which PTH(1-34) amplifies mechanical strain at the cellular interface of osteocytes, and thereby increasing their potential response to dynamic loading. Overall, identifying changes in tissue composition across localized regions plays a key role in understanding the mechanisms that regulate bone strength and its response to loading.

Acknowledgements

This study was supported by grants from the NIH (DE07057, AR056657, and AR064668).

References

[1] J.Y. Rho, L. Kuhn-Spearing, P. Zioupos, Mechanical properties and the hierarchical structure of bone, Med. Eng. Phys. 20 (1998) 92–102.
[2] L.F. Bonewald, The amazing osteocyte, J. Bone Miner. Res. 26 (2011) 229–238.
[3] H. Qing, L.F. Bonewald, Osteocyte remodeling of the perilacunar and pericanalicular matrix, Int. J. Oral Sci. 1 (2009) 59–65.
[4] J.J. Wysolmerski, Osteocytic osteolysis: time for a second look? Bonekey Rep. 1 (2012) 229.
[5] F. Recklinghausen, Untersuchungen uber Rachitis und Osteomalacia, Gustav Fischer, Jena, 1910.
[6] L.F. Belanger, C. Belanger, T. Semba, Technical approaches leading to the concept of osteocytic osteolysis, Clin. Orthop. Relat. Res. 54 (1967) 187–196.
[7] S. Kaya, J. Basta-Pljakic, Z. Seref-Ferlengez, R.J. Majeska, L. Cardoso, T.G. Bromage, Q. Zhang, C.R. Flach, R. Mendelsohn, S. Yakar, S.P. Fritton, M.B. Schaffler, Lactation-induced changes in the volume of osteocyte lacunar-canalicular space alter mechanical properties in cortical bone tissue, J. Bone Miner. Res. 32 (2017) 688–697.
[8] L.F. Belanger, L. Jarry, H.K. Uhthoff, Osteocytic osteolysis in Paget's disease, Rev. Can. Biol. 27 (1968) 37–44.
[9] M.V. Clarke, P.K. Russell, D.M. Findlay, S. Sastra, P.H. Anderson, J.P. Skinner, G.J. Atkins, J.D. Zajac, R.A. Davey, A role for the calcitonin receptor to limit bone loss during lactation in female mice by inhibiting osteocytic osteolysis, Endocrinology 156 (2015) 3203–3214.
[10] B. Hesse, M. Langer, P. Varga, A. Pacureanu, P. Dong, S. Schrof, N. Mannicke, H. Suhonen, C. Olivier, P. Maurer, G.J. Kazakia, K. Raum, F. Peyrin, Alterations of mass density and 3D osteocyte lacunar properties in bisphosphonate-related

osteonecrotic human jaw bone, a synchrotron microCT study, PLoS One 9 (2014) e88481.
[11] S.A. Lloyd, A.E. Loiselle, Y. Zhang, H.J. Donahue, Connexin 43 deficiency desensitizes bone to the effects of mechanical unloading through modulation of both arms of bone remodeling, Bone 57 (2013) 76–83.
[12] H. Qing, L. Ardeshirpour, P.D. Pajevic, V. Dusevich, K. Jahn, S. Kato, J. Wysolmerski, L.F. Bonewald, Demonstration of osteocytic perilacunar/canalicular remodeling in mice during lactation, J. Bone Miner. Res. 27 (2012) 1018–1029.
[13] E.A. Blaber, N. Dvorochkin, C. Lee, J.S. Alwood, R. Yousuf, P. Pianetta, R.K. Globus, B.P. Burns, E.A. Almeida, Microgravity induces pelvic bone loss through osteoclastic activity, osteocytic osteolysis, and osteoblastic cell cycle inhibition by CDKN1a/p21, PLoS One 8 (2013) e61372.
[14] J.D. Gardinier, S. Al-Omaishi, M.D. Morris, D.H. Kohn, PTH signaling mediates perilacunar remodeling during exercise, Matrix Biol. 52–54 (2016) 162–175.
[15] G. Mabilleau, R. Perrot, P.R. Flatt, N. Irwin, D. Chappard, High fat-fed diabetic mice present with profound alterations of the osteocyte network, Bone 90 (2016) 99–106.
[16] K. Tazawa, K. Hoshi, S. Kawamoto, M. Tanaka, S. Ejiri, H. Ozawa, Osteocytic osteolysis observed in rats to which parathyroid hormone was continuously administered, J. Bone Miner. Metab. 22 (2004) 524–529.
[17] E.P. Paschalis, D.B. Burr, R. Mendelsohn, J.M. Hock, A.L. Boskey, Bone mineral and collagen quality in humeri of ovariectomized cynomolgus monkeys given rhPTH(1-34) for 18 months, J. Bone Miner. Res. 18 (2003) 769–775.
[18] E.P. Paschalis, E.V. Glass, D.W. Donley, E.F. Eriksen, Bone mineral and collagen quality in iliac crest biopsies of patients given teriparatide: new results from the fracture prevention trial, J. Clin. Endocrinol. Metab. 90 (2005) 4644–4649.
[19] K. Tai, M. Dao, S. Suresh, A. Palazoglu, C. Ortiz, Nanoscale heterogeneity promotes energy dissipation in bone, Nat. Mater. 6 (2007) 454–462.
[20] H.S. Gupta, W. Wagermaier, G.A. Zickler, D. Raz-Ben Aroush, S.S. Funari, P. Roschger, H.D. Wagner, P. Fratzl, Nanoscale deformation mechanisms in bone, Nano Lett. 5 (2005) 2108–2111.
[21] R.O. Ritchie, The conflicts between strength and toughness, Nat. Mater. 10 (2011) 817–822.
[22] G.R. Brock, J.T. Chen, A.R. Ingraffea, J. MacLeay, G.E. Pluhar, A.L. Boskey, M.C. van der Meulen, The effect of osteoporosis treatments on fatigue properties of cortical bone tissue, Bone Rep. 2 (2015) 8–13.
[23] P.D. Delmas, P. Vergnaud, M.E. Arlot, P. Pastoureau, P.J. Meunier, M.H. Nilssen, The anabolic effect of human PTH (1-34) on bone formation is blunted when bone resorption is inhibited by the bisphosphonate tiludronate–is activated resorption a prerequisite for the in vivo effect of PTH on formation in a remodeling system? Bone 16 (1995) 603–610.
[24] K.M. Chiu, C.D. Arnaud, J. Ju, D. Mayes, P. Bacchetti, S. Weitz, E.T. Keller, Correlation of estradiol, parathyroid hormone, interleukin-6, and soluble interleukin-6 receptor during the normal menstrual cycle, Bone 26 (2000) 79–85.
[25] D.W. Dempster, J.E. Compston, M.K. Drezner, F.H. Glorieux, J.A. Kanis, H. Malluche, P.J. Meunier, S.M. Ott, R.R. Recker, A.M. Parfitt, Standardized nomenclature, symbols, and units for bone histomorphometry: a 2012 update of the report of the ASBMR Histomorphometry Nomenclature Committee, J. Bone Miner. Res. 28 (2013) 2–17.
[26] A. Carden, R.M. Rajachar, M.D. Morris, D.H. Kohn, Ultrastructural changes accompanying the mechanical deformation of bone tissue: a Raman imaging study, Calcif. Tissue Int. 72 (2003) 166–175.
[27] J.A. Timlin, A. Carden, M.D. Morris, R.M. Rajachar, D.H. Kohn, Raman spectroscopic imaging markers for fatigue-related microdamage in bovine bone, Anal. Chem. 72 (2000) 2229–2236.
[28] J.M. Wallace, R.M. Rajachar, M.R. Allen, S.A. Bloomfield, P.G. Robey, M.F. Young, D.H. Kohn, Exercise-induced changes in the cortical bone of growing mice are bone- and gender-specific, Bone 40 (2007) 1120–1127.
[29] C.H. Turner, D.B. Burr, Basic biomechanical measurements of bone: a tutorial, Bone 14 (1993) 595–608.
[30] T. Diab, D. Vashishth, Morphology, localization and accumulation of in vivo microdamage in human cortical bone, Bone 40 (2007) 612–618.
[31] J.S. Yerramshetty, C. Lind, O. Akkus, The compositional and physicochemical homogeneity of male femoral cortex increases after the sixth decade, Bone 39 (2006) 1236–1243.
[32] E. Donnelly, A.L. Boskey, S.P. Baker, M.C. van der Meulen, Effects of tissue age on bone tissue material composition and nanomechanical properties in the rat cortex, J. Biomed. Mater. Res. A 92 (2010) 1048–1056.
[33] A.L. Boskey, E. Donnelly, E. Boskey, L. Spevak, Y. Ma, W. Zhang, J. Lappe, R.R. Recker, Examining the relationships between bone tissue composition, compositional heterogeneity, and fragility fracture: a matched case-controlled FTIRI study, J. Bone Miner. Res. 31 (2016) 1070–1081.
[34] O. Akkus, F. Adar, M.B. Schaffler, Age-related changes in physicochemical properties of mineral crystals are related to impaired mechanical function of cortical bone, Bone 34 (2004) 443–453.
[35] B.R. McCreadie, M.D. Morris, T.C. Chen, D. Sudhaker Rao, W.F. Finney, E. Widjaja, S.A. Goldstein, Bone tissue compositional differences in women with and without osteoporotic fracture, Bone 39 (2006) 1190–1195.
[36] M.D. Morris, G.S. Mandair, Raman assessment of bone quality, Clin. Orthop. Relat. Res. 469 (2011) 2160–2169.
[37] J.L. Holden, J.G. Clement, P.P. Phakey, Age and temperature related changes to the ultrastructure and composition of human bone mineral, J. Bone Miner. Res. 10 (1995) 1400–1409.
[38] J.M. Burnell, E.J. Teubner, A.G. Miller, Normal maturational changes in bone matrix, mineral, and crystal size in the rat, Calcif. Tissue Int. 31 (1980) 13–19.
[39] P. Fratzl, N. Fratzl-Zelman, K. Klaushofer, G. Vogl, K. Koller, Nucleation and growth of mineral crystals in bone studied by small-angle X-ray scattering, Calcif. Tissue Int. 48 (1991) 407–413.
[40] J.T. Swarthout, R.C. D'Alonzo, N. Selvamurugan, N.C. Partridge, Parathyroid hormone-dependent signaling pathways regulating genes in bone cells, Gene 282 (2002) 1–17.
[41] Z.X. Wang, A.A. Lloyd, J.C. Burket, S. Gourion-Arsiquaud, E. Donnelly, Altered distributions of bone tissue mineral and collagen properties in women with fragility fractures, Bone 84 (2016) 237–244.
[42] T.E. Ciarelli, C. Tjhia, D.S. Rao, S. Qiu, A.M. Parfitt, D.P. Fyhrie, Trabecular packet-level lamellar density patterns differ by fracture status and bone formation rate in white females, Bone 45 (2009) 903–908.
[43] M.G. Goff, F.M. Lambers, T.M. Nguyen, J. Sung, C.M. Rimnac, C.J. Hernandez, Fatigue-induced microdamage in cancellous bone occurs distant from resorption cavities and trabecular surfaces, Bone 79 (2015) 8–14.
[44] P. Fratzl, Bone fracture: when the cracks begin to show, Nat. Mater. 7 (2008) 610–612.
[45] G.C. Reilly, Observations of microdamage around osteocyte lacunae in bone, J. Biomech. 33 (2000) 1131–1134.
[46] P. Zioupos, On microcracks, microcracking, in-vivo, in vitro, in-situ and other issues, J. Biomech. 32 (1999) 209–211 (213-59).
[47] G.R. Brock, G. Kim, A.R. Ingraffea, J.C. Andrews, P. Pianetta, M.C. van der Meulen, Nanoscale examination of microdamage in sheep cortical bone using synchrotron radiation transmission x-ray microscopy, PLoS One 8 (2013) e57942.
[48] R. Voide, P. Schneider, M. Stauber, G.H. van Lenthe, M. Stampanoni, R. Muller, The importance of murine cortical bone microstructure for microcrack initiation and propagation, Bone 49 (2011) 1186–1193.
[49] A.R. Bonivtch, L.F. Bonewald, D.P. Nicolella, Tissue strain amplification at the osteocyte lacuna: a microstructural finite element analysis, J. Biomech. 40 (2007) 2199–2206.
[50] J.D. Gardinier, F. Mohamed, D.H. Kohn, PTH signaling during exercise contributes to bone adaptation, J. Bone Miner. Res. 30 (2015) 1053–1063.
[51] T. Sugiyama, L.K. Saxon, G. Zaman, A. Moustafa, A. Sunters, J.S. Price, L.E. Lanyon, Mechanical loading enhances the anabolic effects of intermittent parathyroid hormone (1-34) on trabecular and cortical bone in mice, Bone 43 (2008) 238–248.
[52] L.B. Meakin, H. Todd, P.J. Delisser, G.L. Galea, A. Moustafa, L.E. Lanyon, S.H. Windahl, J.S. Price, Parathyroid hormone's enhancement of bones' osteogenic response to loading is affected by ageing in a dose- and time-dependent manner, Bone 98 (2017) 59–67.
[53] J. Zhang, K.D. Ryder, J.A. Bethel, R. Ramirez, R.L. Duncan, PTH-induced actin depolymerization increases mechanosensitive channel activity to enhance mechanically stimulated Ca2+ signaling in osteoblasts, J. Bone Miner. Res. 21 (2006) 1729–1737.
[54] K.D. Ryder, R.L. Duncan, Parathyroid hormone modulates the response of osteoblast-like cells to mechanical stimulation, Calcif. Tissue Int. 67 (2000) 241–246.
[55] X. Lai, C. Price, S. Modla, W.R. Thompson, J. Caplan, C.B. Kirn-Safran, L. Wang, The dependences of osteocyte network on bone compartment, age, and disease, Bone Res. 3 (2015).
[56] R.D. Ross, M. Mashiatulla, A.G. Robling, L.M. Miller, D.R. Sumner, Bone matrix composition following PTH treatment is not dependent on sclerostin status, Calcif. Tissue Int. 98 (2016) 149–157.
[57] T. Bellido, A.A. Ali, I. Gubrij, L.I. Plotkin, Q. Fu, C.A. O'Brien, S.C. Manolagas, R.L. Jilka, Chronic elevation of parathyroid hormone in mice reduces expression of sclerostin by osteocytes: a novel mechanism for hormonal control of osteoblastogenesis, Endocrinology 146 (2005) 4577–4583.
[58] J.E. Onyia, L.M. Helvering, L. Gelbert, T. Wei, S. Huang, P. Chen, E.R. Dow, A. Maran, M. Zhang, S. Lotinun, X. Lin, D.L. Halladay, R.R. Miles, N.H. Kulkarni, E.M. Ambrose, Y.L. Ma, C.A. Frolik, M. Sato, H.U. Bryant, R.T. Turner, Molecular profile of catabolic versus anabolic treatment regimens of parathyroid hormone (PTH) in rat bone: an analysis by DNA microarray, J. Cell. Biochem. 95 (2005) 403–418.
[59] N.B. Kavukcuoglu, P. Patterson-Buckendahl, A.B. Mann, Effect of osteocalcin deficiency on the nanomechanics and chemistry of mouse bones, J. Mech. Behav. Biomed. Mater. 2 (2009) 348–354.
[60] P.J. Thurner, C.G. Chen, S. Ionova-Martin, L. Sun, A. Harman, A. Porter, J.W. Ager 3rd, R.O. Ritchie, T. Alliston, Osteopontin deficiency increases bone fragility but preserves bone mass, Bone 46 (2010) 1564–1573.